JOURNAL OF SPACECRAFT AND ROCKETS
Vol. 34, No. 5, September–October 1997

Computational Analysis and Validation for Lateral Jet Controlled Missiles

B. Srivastava*
Raytheon Company, Tewksbury, Massachusetts 01876-0901

Comparison of three-dimensional, viscous, turbulent Navier–Stokes simulation for generic missile bodies with wind-tunnel tests have been performed with and without lateral jet thrusters for flow Mach number range of 2–5 and angles of attack of 0–20 deg. Computational results show good overall engineering predictive capability for the surface pressure, normal force coefficient, and jet interaction effects. Further analysis of the computational results shows that the favorable upstream pressure zone (lambda zone) created by the lateral jet, unfavorable pressure loss behind the jet caused by its blockage effect, and the jet wraparound effect are the three principal competing physical mechanisms that inhibit or enhance the jet amplification factor. Canted jet studies to enhance the first of these effects show substantial increase in favorable pressure; however, it does not recover axial component of the thrust vector. Qualitative computations for multijets and hot/binary gas thruster jets have been presented to demonstrate the overall computational capability for missile design applications.

Nomenclature

AF = amplification factor, $1 + (CN_{\text{jet}} - CN_{\text{no-jet}})/(T/q \cdot S)$
CN = normal force coefficient, $(N/q \cdot S)$
dp = pressure differential $(P_{\text{jet}} - P_{\text{no-jet}})/(\text{gamma} \cdot P_{\text{inf}})$
M = freestream Mach number
N = normal force, N (lb)
P = pressure, N/m^2 (lb/ft^2)
q = dynamic pressure, $\frac{1}{2}\rho v^2$
S = missile cross-sectional area, m^2 (ft^2)
T = jet thrust, N (lb)
v = velocity, m/s (ft/s)
y^+ = normal distance from surface in boundary-layer coordinate
α = angle of attack, deg
γ = ratio of specific heats
ρ = density
ϕ = azimuth angle, deg

Subscripts

inf = freestream condition
jet = condition with jet
no-jet = condition with no jet

Introduction

RAPID airframe response time is critical during the homing phase of interceptor missiles. Surface-mounted, fast-reacting jet thrusters offer an attractive alternative to conventional aerodynamic surface control for improved missile agility and maneuverability. Performance enhancements at low speed and high altitude (where dynamic pressure is low) are additional advantages of the surface reaction jets. It has been found that, under some missile orientations and flow conditions, the surface-mounted lateral jet leads to thrust amplification due to a high surface pressure region that forms ahead of the jet on the missile surface. Effective exploitation of the thrust amplification can lead to improved missile performance. However, it has also been observed that at certain other flow conditions and orientations, the reaction jets can produce negative effects, i.e., thrust deamplification. An understanding of the controlling factors that produce high amplification, as well as those that produce low amplification, is critical in developing a credible design basis for optimal missile performance.

Received March 27, 1996; revision received Aug. 14, 1996; accepted for publication Aug. 21, 1996.

*Senior Development Engineer, System Design Laboratory, Raytheon Electronic Systems. Senior Member AIAA.

The problem of the lateral-jet interaction with the external flow, under conditions of varying flight Mach numbers, angles of attack, and jet orientations, is extremely complex in nature and has been studied experimentally and analytically for many years.[1,2] More recently, computational fluid dynamics (CFD) studies[3–7] have been performed to understand these effects. We have adopted an approach that judiciously combines wind-tunnel testing and CFD simulation in an effort to evolve a validated design and analysis tool that can synthesize the physical complexity of the flow and identify its key controlling parameters. This paper deals with the overall CFD validations with and without lateral-jet thrusters and subsequently outlines the utility of the approach by performing several design studies.

This paper is subdivided into several sections. A brief outline of the previous work in this area using CFD approaches is first presented, then details of the computational methodology, grid generation issues, and boundary conditions for the CFD applications are discussed. CFD validation studies for a generic class of missile airframes with and without lateral thrusters are given next. Here wind-tunnel pressure data are compared with the CFD prediction along with the normal forces and amplification factors. The following sections outline CFD application studies dealing with the canted lateral-jet thrusters, flight issues, and the overall summary and conclusions for the paper.

Background

The topic of jet interaction with an external supersonic flow dates back to the mid-1960s,[1,2] when a large number of generic experimental data were generated and related correlation techniques were developed. Emergence of hypersonic interceptors, maturity of CFD, and the advent of supercomputers revived these activities in the late 1980s.[3–7] Several investigators have performed CFD studies for the fundamental problem of jet interaction in relation to adaptive gridding,[8] turbulence models,[9] grid refinements,[10] and the impact of artificial viscosity.[8] These studies range from Euler[11] to Navier–Stokes computations.[12] Of these studies, particular reference is made to the studies reported by Dash et al.[12] and York et al.[6] because much of the current CFD effort is derived from their mature technical expertise in this area. Further details of the methodology and related research work can be obtained from the references cited.

Although a vast number of numerical studies have been performed using controlled jet interaction studies for methodology development, efforts to simulate missile surfaces have been rather limited. More recently, Chan et al.[13] performed a series of studies that lead to the simulation of a full missile surface with control surfaces and jet interaction. Qin and Foster[14] also performed similar studies using a Navier–Stokes approach for an inclined jet on an ogive/cylinder

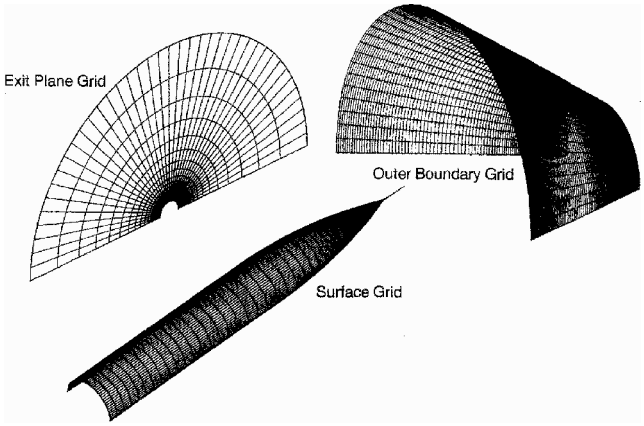

Fig. 1 Grid structure for angle-of-attack simulation.

body. These results depict the remarkable flow details obtained using CFD approaches, which ultimately result in making judicious choices for flight vehicles design and further wind-tunnel testing.

The present paper is aimed at demonstrating the validations aspect of our CFD methodology for a generic missile body, with and without lateral thrusters. Appendages such as wings or tail fins are not included although we are modeling them in our current CFD efforts.

Computational Methodology

PARCH,[6] which is a full Navier–Stokes code with plume/missile airframe steady-flow predictive capability, is being used for our current studies. PARCH code utilizes formulations based on the NASA Ames ARC aerodynamic code and the Arnold Engineering Development Center propulsive extension, PARC. This code is particularly suited for missile surfaces due to its grid patching capability, which is useful for treating embedded surfaces in a flowfield. Patching that is accomplished in mapped computational coordinates is automatically constructed from boundary inputs. Boundary conditions are applied along the outer computational boundaries and relevant embedded surfaces. The code utilizes diagonalized Beam–Warming numerics with matrix-split finite rate chemistry. Several versions of the $K-E$ turbulence model are available in the code that were specifically developed for jet interaction and propulsive studies. We are using capped low Reynolds formulation of Chien's $K-E$ model[12] for the current simulation. Further details of the code capability can be found elsewhere.[6,12]

Typical boundary approaches for the current application (supersonic flows) are specified supersonic freestream conditions at inlet and outer boundaries. Extrapolation procedures are employed at the exit boundary. Surface conditions are appropriate to viscous flows with an adiabatic wall condition. Jet surface boundary condition is the specified supersonic nozzle exit condition.

We are currently using GRIDGEN[15] for grid development, although GENIE[16] was utilized during our initial effort for this application. Figure 1 shows a typical grid for a generic missile body.

Validation Studies

Generic Missile Body

CFD validation plays a crucial role in establishing the level of confidence with which a designer can utilize an analysis tool. Inherent physical models, quality of descretized grid, simulation domain size, and boundary conditions are some of the modeling issues that need to be appropriately addressed to achieve accurate flow predictions. These issues are addressed through detailed validations with wind-tunnel data for a specific application. We have selected the detailed surface pressure measurements conducted at NASA for a circular-arc-cylinder geometry at various flow Mach numbers and angles of attack.[17] Detailed test conditions and geometry for this case can be found in Ref. 17. For this case, the computational grid was $101 \times 51 \times 81$ for half-body with a minimum grid spacing of $y^+ = 5$ near the wall. The test conditions selected for CFD validation were based on our current analysis requirements for various ongoing programs. These conditions are as follows: case 1, angle of attack $\alpha = 0$ and flow Mach numbers $M = 2.3$, 2.96, and 4.63; case 2, $\alpha = 8$ deg and $M = 2.3$ and 4.63; case 3, $\alpha = 16$ deg and $M = 2.96$; and case 4, $\alpha = 20$ deg and $M = 2.96$ and 4.63.

All computations were performed to achieve a reduction of the maximum residual by at least three orders of magnitude. Convergence of the computed results were checked by comparing results for three and four orders of magnitude reduction in the maximum residual. Comparison of the CFD simulations were made with the surface pressure data at the azimuth angles ϕ of 0, 22.5, 45.0, 67.5, 90, 112.5, 135, 157.5, and 180 deg at several axial locations. Typical test results are shown in Figs. 2–9.

Figures 2 and 3 show surface pressure comparisons at a freestream Mach number of 4.6 and an angle of attack of 8 deg. Overall, the computational predictions are within the error bounds for the experiment, as seen in Fig. 2, where various symbols indicate the repeatability level. The experimental data show some asymmetry at higher Mach numbers, as well as large measurement errors at the cone/cylinder juncture. It is observed that comparison on the windward side is excellent. Some discrepancies appear toward the leeward side. These discrepancies could be consistent with physical expectations, i.e., leeward side flow separation would propagate the effect of downstream tunnel conditions on to the body surface. These effects would not be present in free-flight conditions. Better agreement on the leeward side could probably be obtained by utilizing the tunnel downstream pressure as a boundary condition for the CFD flow simulation although this has not been attempted. This trend will be observed for all other comparisons described subsequently.

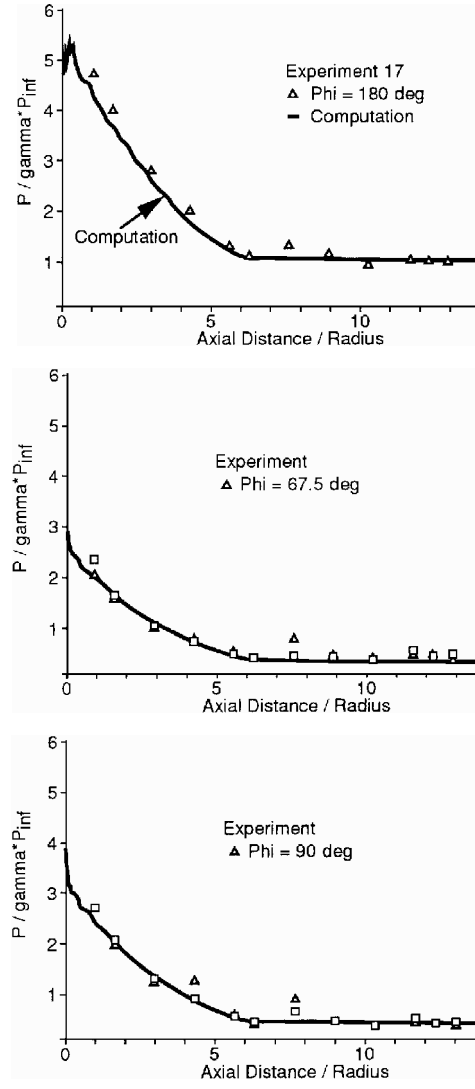

Fig. 2 Comparison of surface pressures at 8-deg angle of attack, $M = 4.6$.

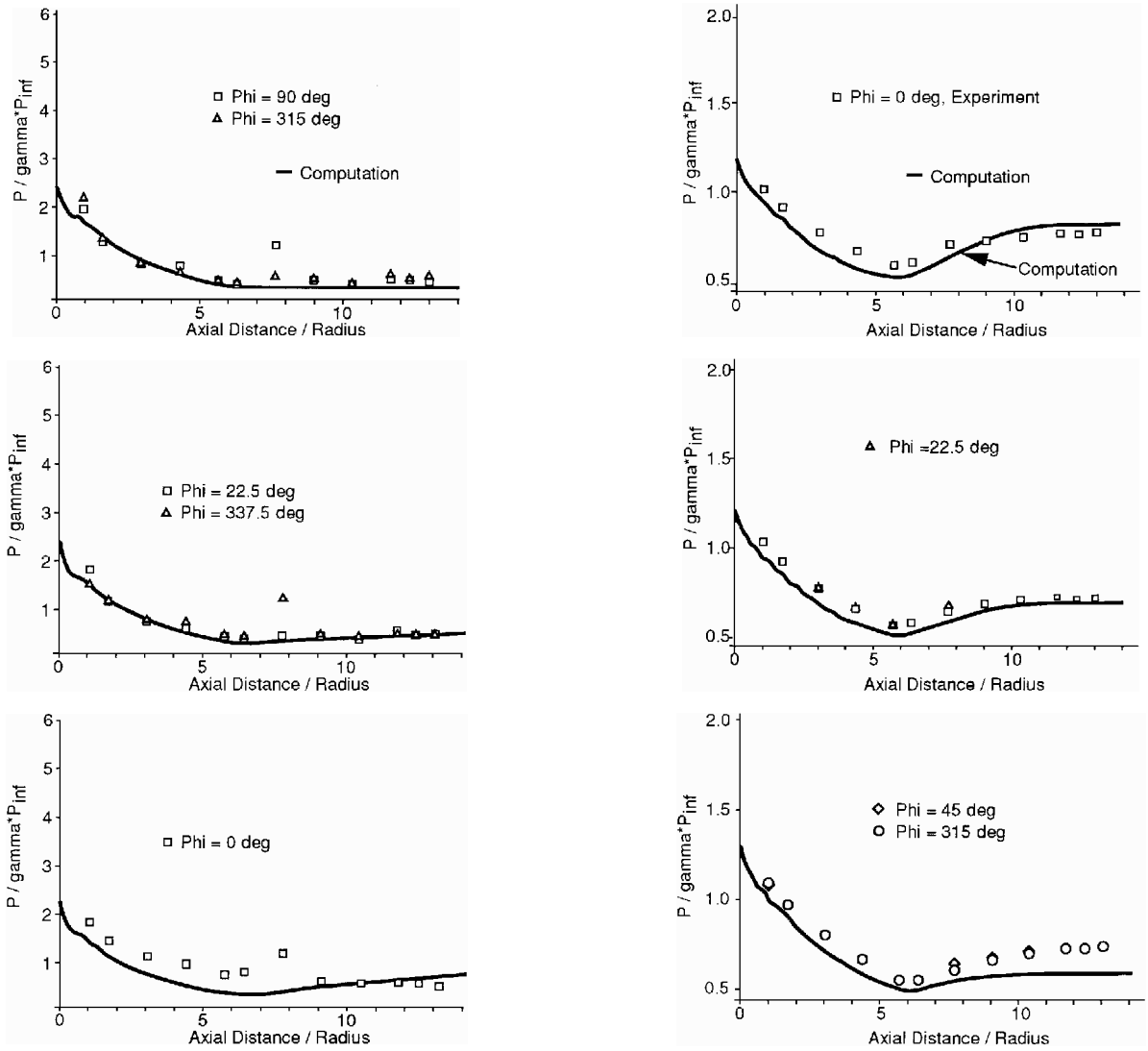

Fig. 3 Comparison of surface pressures at 8-deg angle of attack, $M = 4.6$.

Figures 4 and 5 show comparison at a freestream Mach number of 2.3 at 8-deg angle of attack. Overall behavior remains the same except that, at higher Mach numbers, comparisons are decidedly better. This better comparison is because at higher Mach numbers the leeward side separated zone is thinner and the dominant exit flow is supersonic. The supersonic domain, thus, blocks upstream influence of the downstream tunnel conditions.

At an angle of attack of 20 deg, a large leeward separation zone (low-pressure domain) is expected. Overall pressure comparisons, as depicted in Figs. 6 and 7 for Mach number 2.96, are good. Figures 8 and 9 show similar comparisons at a Mach number of 4.6. Notice from these figures that except at zero ϕ (leeward side symmetry line), comparisons of experimental data with CFD predictions are good.

Lateral Thruster

An understanding of the complex physical interactions associated with the lateral control jet and external aerodynamics for a missile can lead to an improved airframe design. Validated CFD approaches offer an attractive means to achieve this goal. With this objective, we have simulated recent wind-tunnel tests with lateral thrusters using CFD. Specifically, the test case consists of a 2.5 tangent ogive nose geometry with an overall length to diameter ratio of 6.0 at an angle of attack of 20 deg, a flight Mach number of 2.97, and lateral control jet thrusters on the leeward and windward side with thrust ratios of one and four. A circular hole of normalized jet diameter (with missile diameter) 0.1292 located at a normalized distance of 7.312 from the missile nose is used for the jet thruster. The circular area of the jet in the wind-tunnel test is approximated by a square aperture in the CFD simulation. The exit conditions for the nozzle is determined through an iterative solution of isentropic relations, total jet plenum pressure, and jet thrust. The exit conditions are then used as an input to the CFD simulation for jet boundary condition. Computational grid for the missile half-body consists of $211 \times 41 \times 51$ axial, normal, and circumferential points, respectively. The axial points were distributed to resolve the missile nose shape and the jet area. The square jet area was resolved through 10×10 grid points. Turbulent viscous computations were obtained by using a grid point that was placed at y^+, boundary-layer coordinate of five. Successful comparisons have been made with the normal forces,

Fig. 4 Comparison of surface pressures at 8-deg angle of attack, $M = 2.3$.

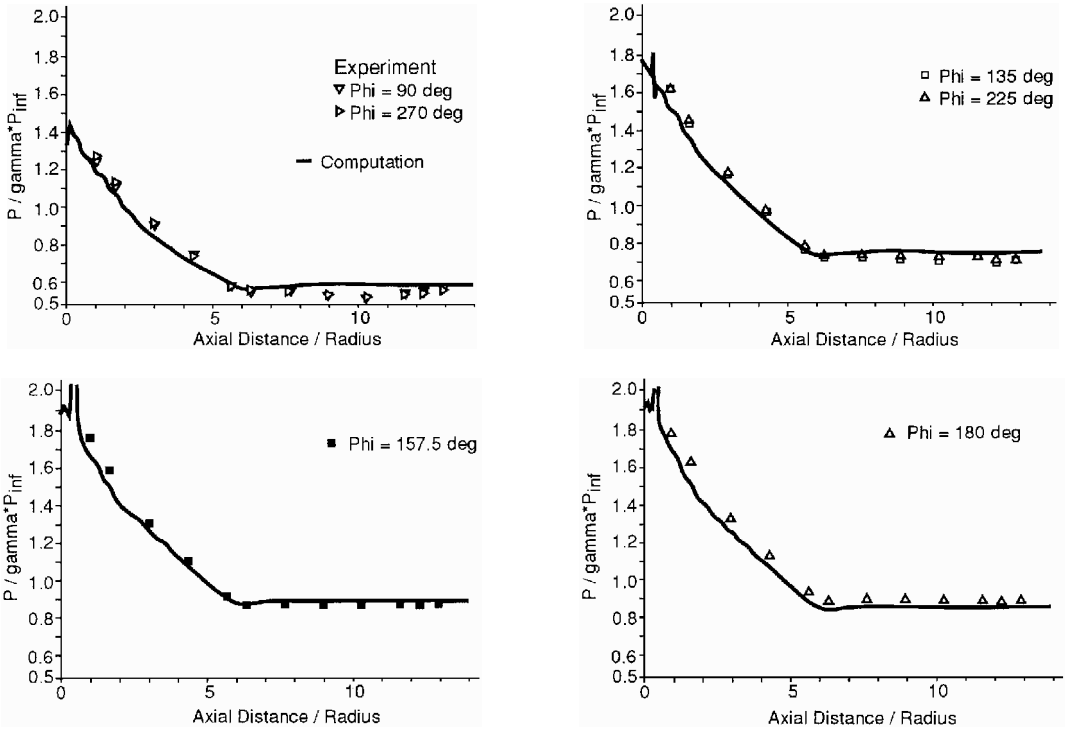

Fig. 5 Comparison of surface pressures at 8-deg angle of attack, $M = 2.3$.

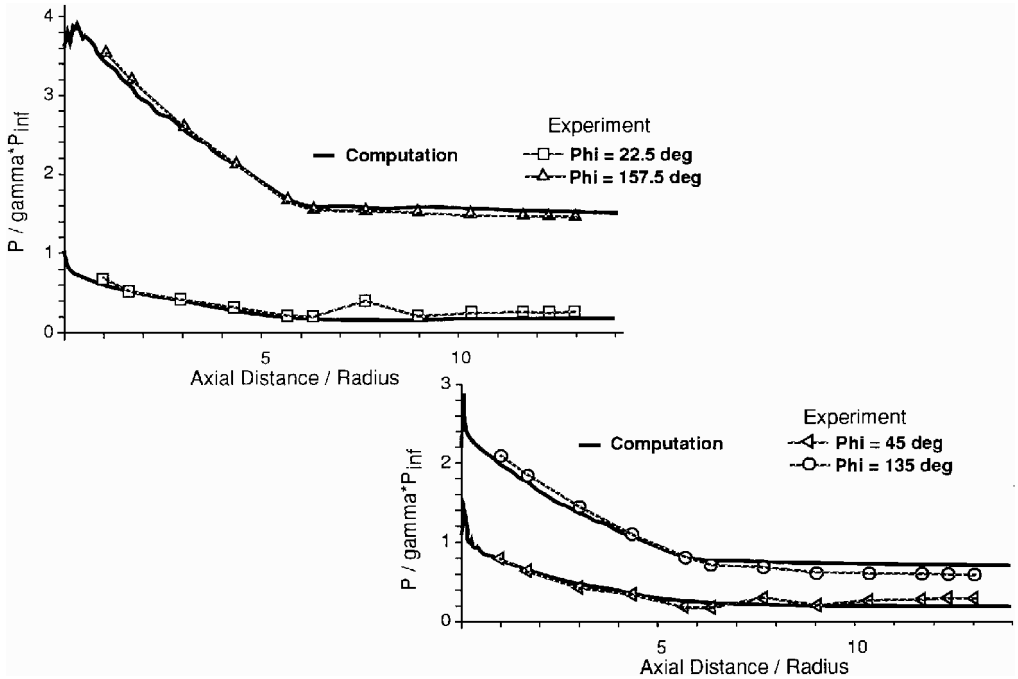

Fig. 6 Comparison of surface pressures at 20-deg angle of attack, $M = 2.96$.

amplification factors, and pressure sensitive paint (PSP) data. Some of these results are described as in the following.

Test Cases

Five test cases were identified for CFD simulation. For all cases, the freestream Reynolds number was 8.2×10^5 based on the missile radius. These test cases are described next.

Case 1

The flow Mach number is 2.97, angle of attack 20 deg, jet thrust ratio $(T/q \cdot S)$ 1.0, and leeward jet location ϕ 0 deg. The data available are force and moment coefficients, amplification factor, and PSP data. T is the jet thrust in pounds, q is the dynamic head, and S is the cylinder cross-sectional area.

Case 2

The flow Mach number is 2.97, angle of attack 20 deg, jet thrust ratio $(T/q \cdot S)$ 1.0, and windward jet location ϕ 180 deg. The data available are force and moment coefficients, amplification factor, and PSP data.

Case 3

The flow Mach number is 2.97, angle of attack 20 deg, jet thrust ratio $(T/q \cdot S)$ 4.0, and leeward jet location ϕ 0 deg. The data available are force and moment coefficients, amplification factor, and PSP data.

Case 4

The flow Mach number is 2.97, angle of attack 20 deg, jet thrust ratio $(T/q \cdot S)$ 4.0, and windward jet location ϕ 180 deg. The data

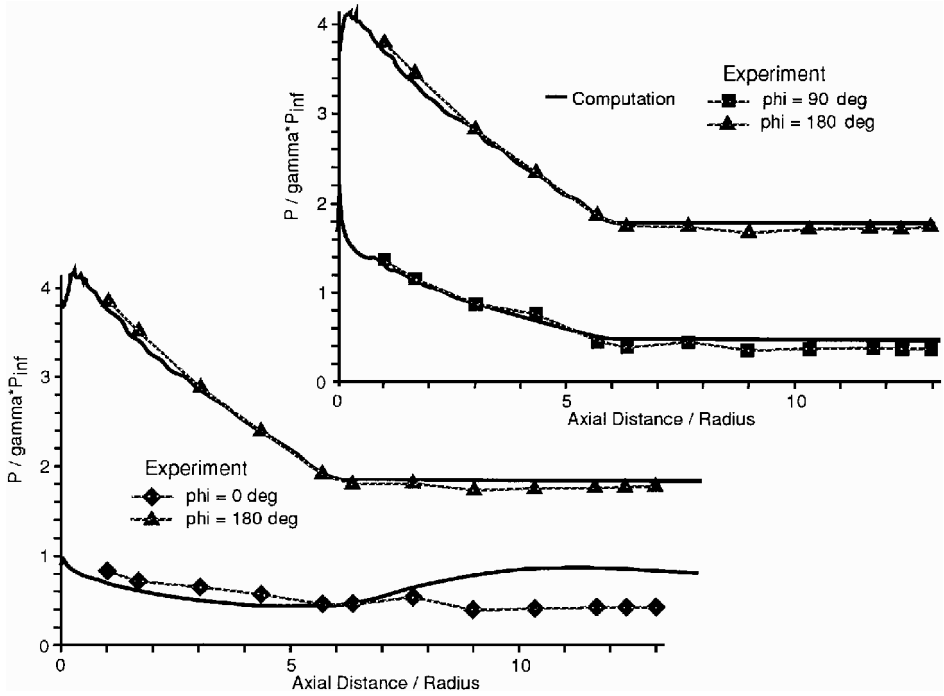

Fig. 7 Comparison of surface pressures at 20-deg angle of attack, $M = 2.96$.

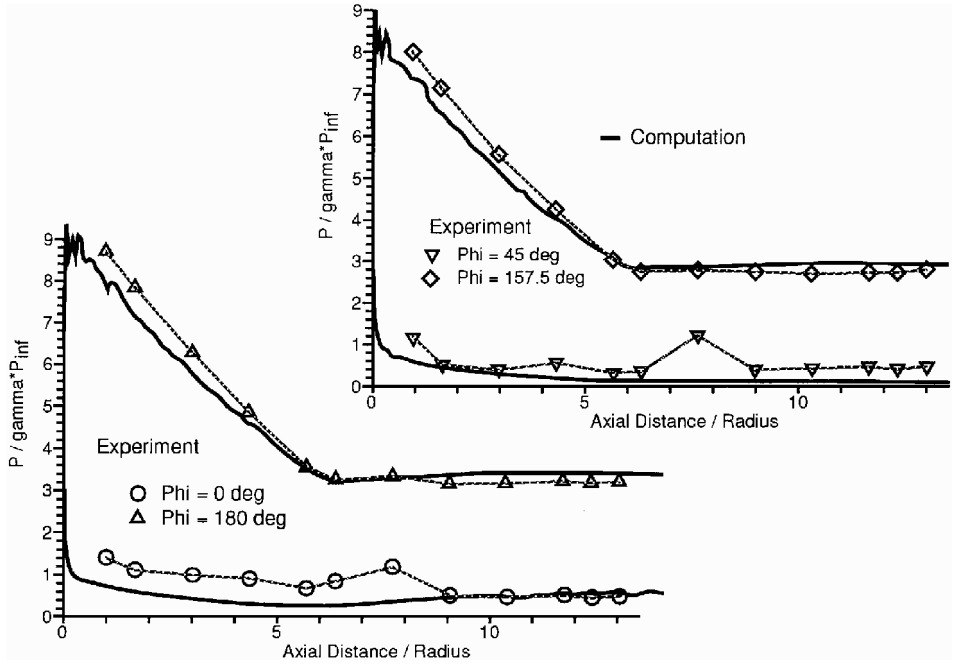

Fig. 8 Comparison of surface pressures at 20-deg angle of attack, $M = 4.63$.

available are force and moment coefficients, amplification factor, and PSP data.

Case 5

The flow Mach number is 2.97, angle of attack 20 deg; there is no jet case. The data available are force and moment coefficients, amplification factor, and PSP data.

Procedure

Although the wind-tunnel tests were carried out with tail fins installed on the model, schedule constraints precluded their inclusion in this CFD effort. However, since the tail panels were fully instrumented in the wind-tunnel tests, their measured loads and an estimate of the tail-to-body interference load (using conventional interference estimate such as those utilized in aerodynamic codes) can be removed from the airframe measured load. This procedure yields an estimate of the load on the body alone, i.e., as though the body were tested without tail panels. The resulting estimate was used for comparison with the CFD results. This technique introduces an uncertainty that is difficult to quantify, especially since the tail-to-body interference is difficult to estimate in the presence of the thruster. Analysis of the CFD results indicate supersonic external flows for these conditions, and thus this procedure will not introduce errors on the missile body except near the tail.

Available PSP data and amplification factors (derived from the balance data) were also included for comparisons. The objective was to assess the relative accuracy of the CFD predictions as compared to the test data. No repeat runs were made to improve CFD predictions, and all comparisons were made after the reduction of maximum residual by three orders of magnitude. No attempt was made to

study the impact of dissipative parameters or varying turbulence models on the predicted results.

Comparisons

Comparisons of the measured and computed normal force and amplification factors are shown in Table 1.

The overall comparisons between the CFD predictions and experiment are reasonable, especially for parameter trend behavior.

Discussion

Figure 10 shows the symmetry plane pressure contour for case 5, the baseline flow pattern without the lateral thruster. Compare this with Fig. 11, windward jet thruster of case 4. One can observe the structure in front of the jet thruster, a zone of high pressure ahead of the jet followed by a massive blockage of the windward side of the missile surface. Note that, in this orientation, the loss of positive surface pressure behind the jet must be overbalanced by the gain in positive pressure ahead of the jet to achieve an amplification of the thrust, i.e., $AF > 1$. However, the positive high-pressure domain ahead of the jet, even though intense in its peak, is confined to a very small region resulting in $AF < 1$. This effect is more strongly evident if one observes the surface pressure differential between the jet-on and jet-off conditions for the entire missile surface, as shown in Fig. 12, i.e., surface pressure differential between cases 4 and 5. Figure 12 represents the difference in surface pressure caused solely by the thruster jet. For this case the integrated effect of this difference is not favorable, resulting in $AF < 1$. Pressure contours for the thruster on the leeward side symmetry plane are shown in Fig. 13. In this case, the thruster exhausts into a vortical flow region resulting in a less affected plume. Because the local dynamic head is low on the leeward side, the lateral jet creates a larger region of increased pressure ahead of itself. This is clearly seen in Fig. 14, where the surface pressure differential between the jet off and jet on is shown for the leeward jet. This effect yields a somewhat marginal gain in amplification factor for this orientation.

Application Studies

Effect of Jet Angle

A critical evaluation of the CFD results shows that, for a normal jet, favorable pressures are created just ahead of the thruster jet, whereas adverse pressures are created behind the jet. The net effect of these two domains dictates the magnitude of the amplification factors. Thus, a designer's goal would be to maximize favorable pressure domain and minimize adverse pressure domain to enhance the amplification factors. One way to achieve this is with a forward inclined thruster jet.

Leeward Jet

Figure 14 shows the surface pressure differential ($\Delta p = p_{\text{jet}} - p_{\text{no-jet}}$, where pressure is normalized as $p/\gamma \cdot p_{\infty}$) for a leeward jet at an angle of attack of 20 deg, Mach number 2.97, and a thrust ratio of four for a normal jet. It shows all basic flow structures and wraparound of the jet. Figure 14 can now be compared to Fig. 15, which is for a 30-deg forward inclined jet. Notice that the extent of favorable pressure increases significantly for the 30-deg forward inclined jet. This increase in favorable pressure is a desirable effect, sought for in our design goals. However, notice from Table 2 that the integrated effect, when referenced to the total component of the thrust, does not show a significant gain in the amplification factor. This lack of significant gain in amplification factor is because of the static thrust loss due to the cosine of the jet inclination angle.

Windward Jet

Amplification factors tend to reduce significantly for the windward jet due to jet induced wake aft of the jet on the missile body.

Table 1 Comparison of amplification factors

Test case	CN[a] test	CN CFD	AF[b] test	AF CFD
1	3.37	2.77	0.97	0.9
2	4.64	4.56	0.28	0.6
3	0.21	−0.19	0.96	1.07
4	7.33	7.27	0.76	0.9
5	4.36	3.73	——	——

[a]Normal force coefficient $= N/q \cdot S$, where N is the normal force.
[b]Amplification factor $= 1 +$ interactive aeroforce/thrust.

Table 2 CFD predicted amplification factors[a] for several jet angles

Jet angle ϕ[b]	Thrust ratio[c] = 1.0 Windward jet	Thrust ratio[c] = 1.0 Leeward jet	Thrust ratio[c] = 4.0 Windward jet	Thrust ratio[c] = 4.0 Leeward jet
30	0.5		0.61	0.75
45	0.64	1.01	——	——
90	0.60	0.9	0.9	1.07
135	0.37			

[a]Amplification factor defined with total component of the thrust.
[b]Forward jet is defined for $\phi < 90$ deg.
[c]Thrust ratio defined with the total component of the thrust.

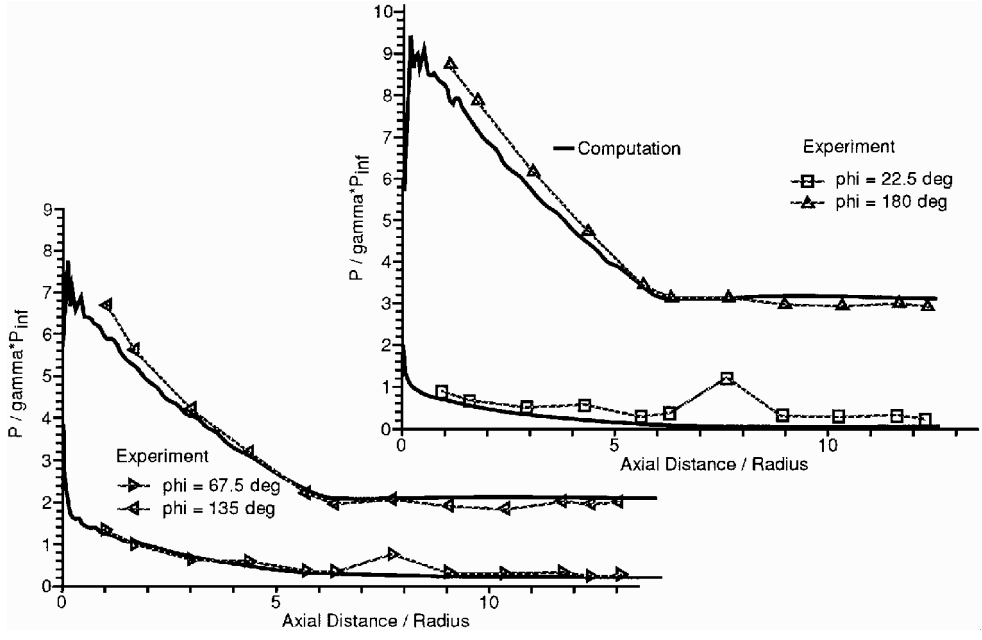

Fig. 9 Comparison of surface pressures at 20-deg angle of attack, $M = 4.63$.

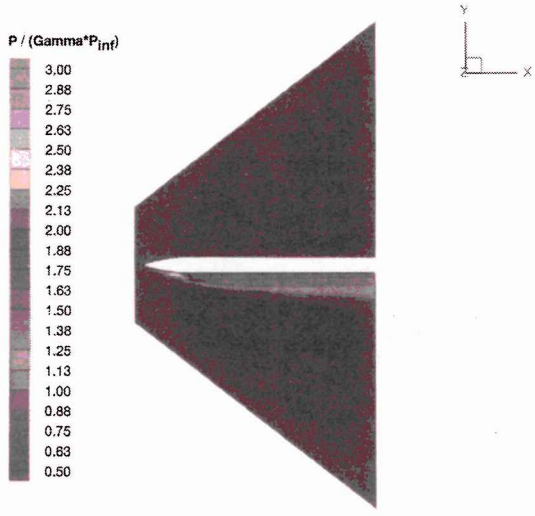

Fig. 10 Pressure contours on the symmetry plane for jet-off case: M = 2.97 and α = 20.0.

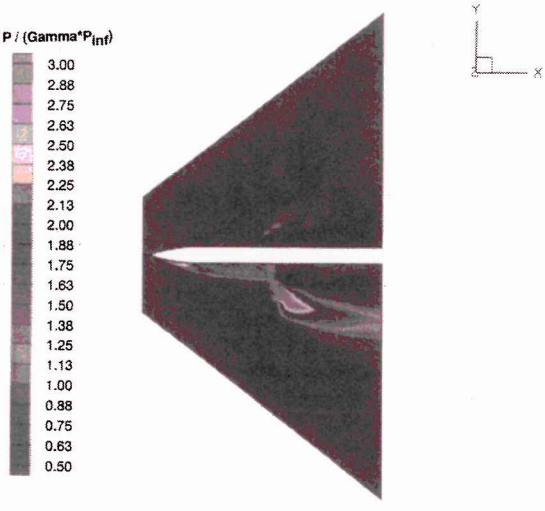

Fig. 11 Pressure contours on the symmetry plane for windward jet: M = 2.97, α = 20.0 deg, and $T/q \cdot s$ = 4.0.

Fig. 12 Surface pressure differential for normal windward jet and jet-off conditions.

This effect is seen in Fig. 12 for a windward jet at Mach number 2.97, angle of attack of 20 deg, and thrust ratio of four. Figure 16 shows a case of a forward 30-deg lateral jet on the windward side. Whereas there are visible changes in the flow structure, the effect is not so pronounced as was observed for the leeward jet case. However, notice that the jet angle has a definite desirable effect when forward jets are employed on the windward side as compared to the normal jets. This apparent gain, however, does not reflect significantly in

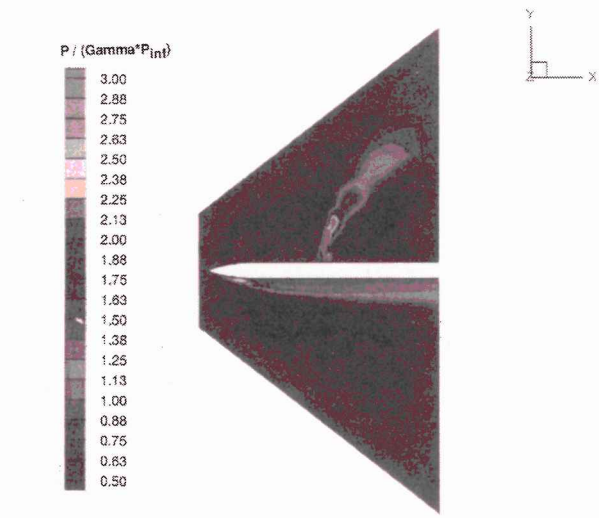

Fig. 13 Pressure contours on the symmetry plane for leeward jet: M = 2.97, α = 20.0 deg, and $T/q \cdot s$ = 4.0.

Fig. 14 Surface pressure differential for normal leeward jet and jet-off conditions.

Fig. 15 Surface pressure differential for 30-deg forward leeward jet and jet-off conditions.

the amplification factor that is referenced to the total thrust as shown in Table 2. Again, the cosine of the jet inclination angle accounts for this behavior.

Thrust Ratio

The gain of favorable pressures for the forward inclined jets on the windward side is enhanced when the thrust ratio is increased. However, this gain in the favorable pressure is unable to overcome the cosine effect, which increases significantly at higher thrust levels.

Fig. 16 Surface pressure differential for 30-deg windward forward jet and jet-off conditions.

Table 2 shows that the amplification factor defined on the basis of total thrust would decrease at higher thrust ratios as compared to a normal jet case. The CFD computed amplification factors for all of the cases described are shown in Table 2. This table shows that the amplification factor defined on the basis of total thrust shows only a marginal increase at the lower thrust levels and a decrease at higher thrust levels. This behavior is primarily caused by the cosine effect of the jet inclination angle.

Thruster Jet-External Aerodynamics Interaction Physics

Based on the CFD studies outlined, three important physical mechanisms are identified that control the overall amplification factor for a missile.

Jet-Induced Wake

The jet acts as a blunt body to the incoming flow, causing a massive wake, which works as an adverse effect for all cases of the control jet location. Because of this effect additional forces are generated that are undesirable. Jet-induced wake is a very dominant effect when the control jet is on the windward side.

Lambda Effect

Lambda effect happens forward of the jet. Primarily, a lead shock followed by other shocks and expansions ahead of the jet are formed that tend to increase the surface pressures. These are favorable effects, and their extent is dependent on the flow conditions and jet angle.

Wraparound Effect

The jet wraparound effect has been observed with a windward jet. Essentially, the high momentum of the incoming flow creates a skewed shape of the jet that tends to reach over to the leeward side, increasing the leeward surface pressure. This is again an undesirable effect. Figures 17–19 show these effects, where surface pressures are plotted against axial position for various circumferential locations on the missile surface. Notice from Fig. 17 that, without a jet, the surface pressures asymptote to a certain value on the missile surface. Compare this with Fig. 18, which has a leeward jet (located near $J = 1$). Notice that the pressures forward of the jet (jet located at $X = 14.6$) increase, which ultimately asymptotes to a lower value on the leeward side. In contrast, the windward surface pressures for this case are unchanged. On the other hand, a windward jet under identical conditions is seen (in Fig. 19) to affect the leeward locations significantly. Thus, the loss of high pressure on the windward side due to the blockage and the increase of pressure on the leeward side due to the wraparound effect act together to yield much larger undesirable effects for this case than for the leeward jet.

Flight Vehicle Considerations

Although the primary conclusions derived based on wind-tunnel data and the CFD studies for body alone with a single jet are likely to remain same, the magnitudes may somewhat vary because of the following effects: 1) multijets on the missile surface, 2) hot binary gas mix for the lateral jet, and 3) effect of wings.

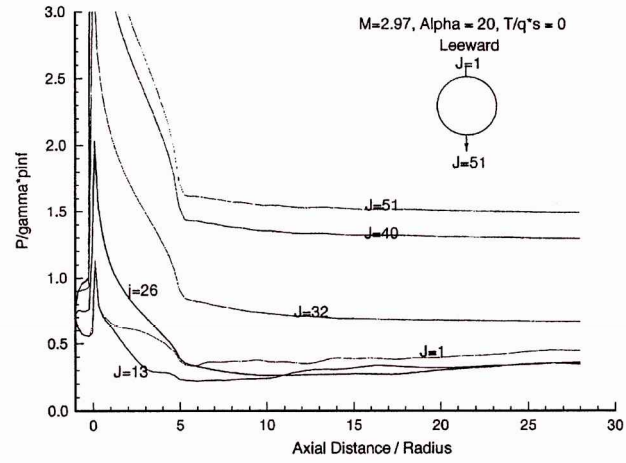

Fig. 17 Axial pressure variation for several circumferential angles without jet.

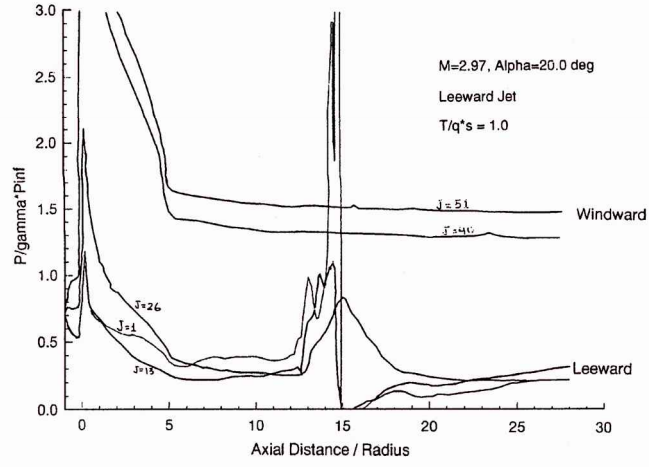

Fig. 18 Axial surface pressure variation for several circumferential angles with leeward jet.

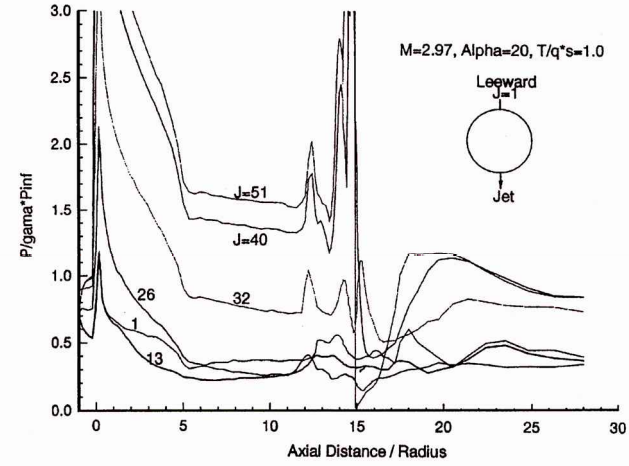

Fig. 19 Axial surface pressure variation for several circumferential angles with windward jet.

These effects have not been fully investigated using our current capabilities. However, preliminary trend studies do not show any significant deviation from our major conclusions. Figures 20–22 show multijet effects, temperature field, and streamlines for a generic missile surface without wings. Note from Fig. 20 the four multijets (this case was for four circumferential jets at zero angle of attack); the jet interfaces tend to inhibit the wraparound effects of the jet, thereby channeling the flow. Figures 21 and 22 are temperature and streamline plots for the same case.

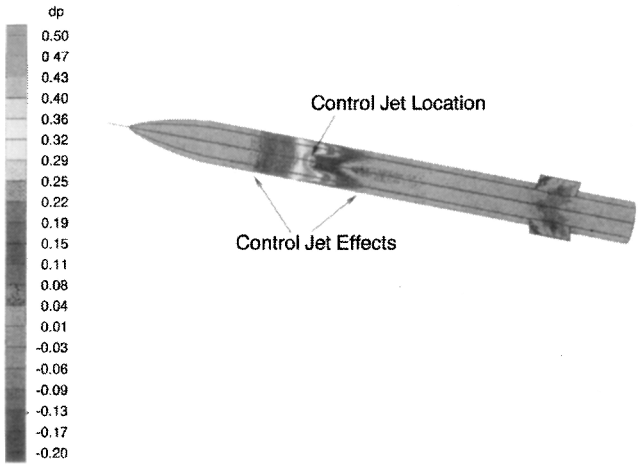

Fig. 20 Missile surface pressure differential for jet-on and jet-off cases for multiple jets: $M = 2.5$ and $\alpha = 0.0$.

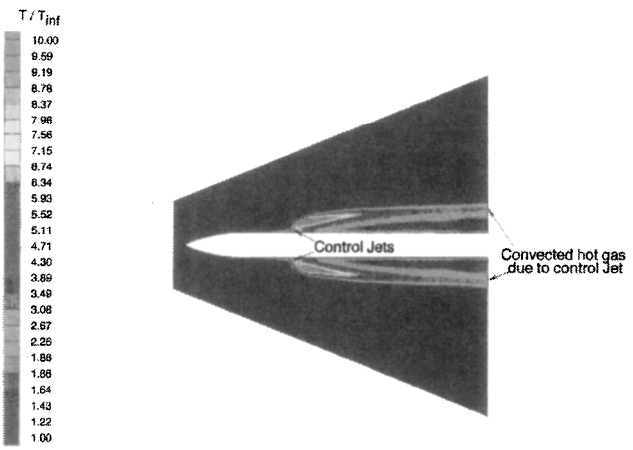

Fig. 21 Temperature field in external flow with hot gas control jets: $M = 2.5$ and $\alpha = 0.0$.

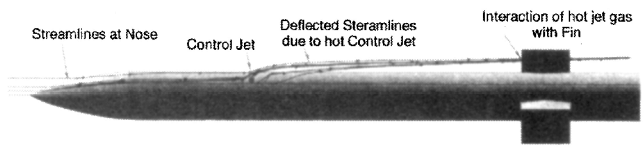

Fig. 22 Streamlines showing interaction of control jet with external aerodynamics: freestream Mach number $M = 2.5$ and $\alpha = 0.0$ deg.

Summary and Conclusions

Extensive tests of the PARCH code with NASA wind-tunnel pressure measurements show good predictive capability for a generic missile body. Further extensive comparisons of the code with Raytheon's wind-tunnel measurements have been performed for a missile at 20-deg angle of attack, flow Mach number of 2.97, and lateral control jet with thrust ratios of 1.0 and 4.0. Normal force coefficients and amplification factors obtained from wind-tunnel measurements compare well with the CFD predictions.

Synthesis of the CFD generated results has been performed to identify possible physical mechanisms that inhibit the potential gain in amplification factors for leeward and windward located control jets on a missile surface. Based on this, design studies have been performed to demonstrate that forward inclined jets create favorable pressure effects whose magnitude is dependent on the flight conditions and jet characteristics. However, these effects do not recover the loss of thrust vector (component that appears as drag) due to jet inclination on the missile surface.

Preliminary qualitative computations for multijets, hot/binary mixture thruster jet gas, and a full missile geometry including control surfaces suggest no inherent limitation of the PARCH code for our near future missile applications.

References

[1]Cassel, L. A., Davis, J. G., and Engh, D. P., "Lateral Jet Control Effectiveness Prediction for Axisymmetric Missile Configurations," U.S. Army Missile Command, Rept. RD-TR-68-5, Redstone Arsenal, AL, June 1968.

[2]Spring, D., "An Experimental Investigation of the Interference Effects due to a Lateral Jet Issuing from a Body of Revolution over the Mach No. Range of 0.8 to 4.5," U.S. Army Missile Command, Rept. RD-TR-68-10, Redstone Arsenal, AL, Aug. 1968.

[3]Chamberlain, R., "Control Jet Interaction Flowfield Analysis," *Aerodynamic Investigations*, Vol. 5, Feb. 1990 (Lockheed Rept. LMSC F268936).

[4]Chamberlain, R., "Calculation of Three-Dimensional Jet-Interaction Flowfields," AIAA Paper 90-2099, 1990.

[5]Weatherly, D., and McDonough, J., "Performance Comparisons of Navier–Stokes Codes for Simulating Three-Dimensional Hypersonic Crossflow/Jet Interaction," AIAA Paper 91-2096, 1991.

[6]York, B. J., Sinha, N., Kenzakowski, D. C., and Dash, S. M., "PARCH Code Simulation of Tactical Missile Plume/Airframe/Launch Interactions," *19th JANNAF Exhaust Plume Technology Meeting*, 1991, pp. 645–674 (CPIA PWB 568).

[7]Chan, S. C., Roger, R. P., Edwards, G. L., and Brooks, W. B., "Integrated Jet Interactions CFD Predictions and Comparison to Force and Moment Measurements for a Thruster Attitude Controlled Supersonic Missile," AIAA Paper 93-3522, 1993.

[8]Lytle, J. K., Harloff, G. J., and Hsu, A. T., "Three-Dimensional Compressible Jet-in-Crossflow Calculations Using Improved Viscosity Models and Adapted Grid," AIAA Paper 90-2100, 1990.

[9]Dash, S. M., Sinha, N., York, B. J., Lee, R. A., and Hosangadi, A., "On the Inclusion of Advanced Turbulence Models and Nonequilibrium Thermochemistry into State-of-the-Art CFD Codes and Their Validation," AIAA Paper 92-2764, 1992.

[10]Rizzetta, D. P., "Numerical Simulation of Slot Injection into a Turbulent Supersonic Stream," AIAA Paper 92-0827, 1992.

[11]Darmieux, M., and Marasaa-Poey, R., "Numerical Assessment of Aerodynamic Interactions on Missiles with Transverse Jets Control," AGARD Meeting on Computational and Experimental Assessment of Jets in Cross Flow, April 1993.

[12]Dash, S. M., York, B. J., Sinha, N., Lee, R. A., Hosangadi, A., and Kenzakowski, D. C., "Recent Developments in the Simulation of Steady and Transient Transverse Jet Interactions for Missile, Rotorcraft, and Propulsive Applications," AGARD Meeting on Computational and Experimental Assessment of Jets in Cross Flow, 1993, pp. 29-1, 29-21.

[13]Chan, S. C., Roger, R. P., Brooks, W. B., Edwards, G. L., and Boukather, S. B., "CFD Predictions and Comparisons to Wind Tunnel Data for the Asymmetric Firing of a Forward Mounted Attitude Control Thruster," AIAA Paper 95-1895, June 1995.

[14]Qin, N., and Foster, G. W., "Study of Flow Interactions due to a Supersonic Lateral Jet Using High Resolution Navier–Stokes Solutions," AIAA Paper 94-2151, June 1995.

[15]Steinbrenner, J. P., and Chawner, J. R., "Recent Enhancements to the GRIDGEN Structural Grid Generation System," *Proceedings of the NASA Workshop on Software Systems for Surface Modeling and Grid Generation*, Hampton, VA, 1992.

[16]Soni, B. K., Thompson, J. F., Stokes, M. L., and Shih, M. H., "GENIE^{++}, EAGLEVIEW and TIGER: General Purpose and Special Purpose Graphically Interactive Grid System," AIAA Paper 92-0071, Jan. 1992.

[17]Landrum, E. J., "Wind Tunnel Pressure Data at Mach Numbers 1.6 to 4.64 for a Series of Bodies of Revolution at Angles of Attack from −4 deg to 60 deg," NASA TM X-3558, Oct. 1977.

T. C. Lin
Associate Editor